Accessibility of the Distal Heme Face, Rather than Fe−His Bond Strength, Determines the Heme-Nitrosyl Coordination Number of Cytochromes *c*′: Evidence from Spectroscopic Studies†

Colin R. Andrew,*,‡ Lenord J. Kemper,‡ Tammy L. Busche,‡ Arianne M. Tiwari,‡ Michael C. Kecskes,‡ James M. Stafford,‡ Lea C. Croft,‡ Shen Lu,§ Pierre Moënne-Loccoz,§ Willa Huston,|| James W. B. Moir,|| and Robert R. Eady⊥

Department of Chemistry & Biochemistry, Eastern Oregon University, La Grande, Oregon 97850, Department of Environmental & Biomolecular Systems, OGI School of Science & Engineering, Oregon Health & Science University, Beaverton, Oregon 97006, Department of Biology, University of York, U.K., and Department of Biological Chemistry, John Innes Centre, Norwich, U.K.

Received March 7, 2005; Revised Manuscript Received April 17, 2005

ABSTRACT: The heme coordination chemistry and spectroscopic properties of *Rhodobacter capsulatus* cytochrome *c*′ (RCCP) have been compared to data from *Alcaligenes xylosoxidans* (AXCP), with the aim of understanding the basis for their different reactivities with nitric oxide (NO). Whereas ferrous AXCP reacts with NO to form a predominantly five-coordinate heme-nitrosyl complex via a six-coordinate intermediate, RCCP forms an equilibrium mixture of six-coordinate and five-coordinate heme-nitrosyl species in approximately equal proportions. Ferrous RCCP and AXCP both exhibit high Fe−His stretching frequencies (227 and 231 cm^{-1}, respectively), suggesting that factors other than the Fe−His bond strength account for their differences in heme-nitrosyl coordination number. Resonance Raman spectra of ferrous-nitrosyl RCCP confirm the presence of both five-coordinate and six-coordinate heme-NO complexes. The six-coordinate heme-nitrosyl of RCCP exhibits a fairly typical Fe−NO stretching frequency (569 cm^{-1}), in contrast to the relatively high value (579 cm^{-1}) of the AXCP six-coordinate heme-nitrosyl intermediate. It is proposed that NO experiences greater steric hindrance in binding to the distal face of AXCP, as compared to RCCP, leading to a more distorted Fe−N−O geometry and an elevated Fe−NO stretching frequency. Evidence that RCCP has a more accessible distal coordination site than in AXCP stems from the fact that ferric RCCP readily forms a heme complex with exogenous imidazole, whereas AXCP does not. A model is proposed in which distal heme-face accessibility, rather than the proximal Fe−His bond strength, determines the heme-nitrosyl coordination number in cytochromes *c*′.

The coordination of nitric oxide (NO) to protein heme centers is important to a variety of physiological processes including NO metabolism and signal transduction (*1*−*3*). In the case of ferrous heme-NO complexes, two broad classes exist: those having a six-coordinate heme nitrosyl (6c-NO) with NO bound opposite an endogenous amino acid ligand, and those having a five-coordinate heme nitrosyl (5c-NO) in which the axial covalent link to the protein is severed by NO binding. Whether or not the endogenous ligand remains bound to a ferrous heme-nitrosyl complex is a major factor controlling the reactivity of the bound NO as well as any functional effects produced upon NO binding. For example, in soluble guanylate cyclase (sGC), structural changes resulting from 5c-NO formation (and the associated Fe−His bond cleavage) are believed to trigger cyclase activity, leading to increased cGMP levels and a resultant signal cascade (*1*, *4*, *5*).

Previous studies of hemoproteins have suggested that the tendency to form 5c-NO (rather than 6c-NO) complexes is governed by the Fe−His bond strength, and that this is reflected in the frequency of the Fe−His stretching vibration, ν(Fe−His), determined by resonance Raman (RR) spectroscopy in the five-coordinate ferrous state (5c-Fe^{2+}) (*6*). A ν(Fe−His) frequency of ∼210 cm^{-1} has been proposed as the cutoff value below which NO is able to cleave the Fe−His bond to form a 5c-NO species, and above which the Fe−His bond remains intact to yield a 6c-NO adduct (*6*). However, several RR studies have reported data that do not fit this correlation. For example, bacterial cytochromes *c*′ exhibit high ν(Fe−His) frequencies of ∼230 cm^{-1} (*7*, *8*), yet vary greatly in their tendency toward forming 5c-NO and 6c-NO complexes (*9*). In addition, an sGC-like protein from the prokaryote *Vibrio cholerae* generates a 5c-NO species despite exhibiting a ν(Fe−His) frequency of 224

† C.R.A. gratefully acknowledges support from the EOU Faculty Scholars Program, EOU Foundation, and the National Science Foundation (Grant MCB-0417152).

* To whom correspondence should be addressed. One University Boulevard, Eastern Oregon University, La Grande, OR 97850-2899. E-mail: candrew@eou.edu. Phone: (541) 962-3322. Fax: (541) 962-3873.

‡ Eastern Oregon University.

§ Oregon Health & Science University.

|| University of York.

⊥ John Innes Centre.

10.1021/bi050428g CCC: $30.25
Published on Web 05/26/2005

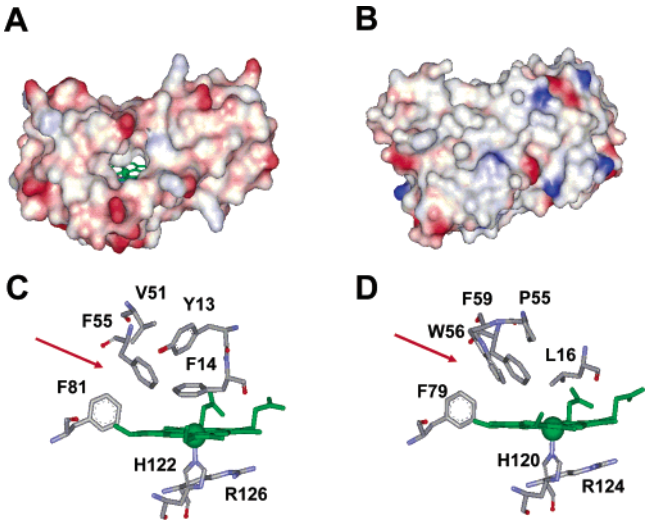

FIGURE 1: Structural representations of cytochrome *c*′ protein subunits and their ferric heme environments. Protein van der Waals surfaces of (A) RCCP and (B) AXCP show that only RCCP has a solvent accessible channel to the distal heme (shown in green). The immediate heme environments of (C) RCCP and (D) AXCP both have relatively crowded hydrophobic distal pockets. An arrow indicates the direction of ligand access from solution. Image prepared with WebLab ViewerLite v4.0 using structural coordinates from refs *25* and *30*.

cm^{-1} in its 5c-Fe^{2+} state (*10*). These examples of apparently anomalous NO-binding behavior suggest that there may be instances when the heme-nitrosyl coordination number is determined by factors other than the Fe−His bond strength.

Cytochromes *c*′ are a group of class IIa cytochromes found in certain types of proteobacteria (*11*, *12*). The exact role of cytochromes *c*′ is still unclear, although recent studies have suggested that NO binding at their heme centers may be physiologically relevant (*13*−*19*). Complete amino acid sequences have been reported for a variety of cytochromes *c*′ from different organisms (see (*20*)), along with a number of X-ray crystal structures (see, for example, refs *21*−*24* and references therein). Most cytochromes *c*′ are homodimers with each subunit (∼14 kD) containing a pentacoordinate heme center (see Figure 1). The proximal heme environments of all cytochromes *c*′ contain a proximal His ligand, together with a Lys or Arg residue located four residues after the heme-binding motif, Cys-X-X-Cys-His. Access to the hydrophobic distal heme pocket is hindered by noncoordinated residues. Tahirov et al. have classified cytochromes *c*′ into two groups based on the nature of their distal heme pockets. Members of group 1 possess an aromatic residue (Phe or Tyr) above the distal heme coordination site, combined with a solvent exposed channel to the distal heme pocket. In contrast, group 2 cytochromes *c*′ have an aliphatic residue (Leu or Met) above the distal coordination site, and the distal pocket is not directly exposed to solvent.

Recent interest surrounds the discovery of novel heme coordination chemistry in *Alcaligenes xylosoxidans* cytochrome *c*′ (AXCP). In particular, ferrous AXCP reacts with NO to form a distal 6c-NO intermediate that subsequently converts to a 5c-NO product with an unprecedented proximal coordination of NO at the site originally occupied by the His ligand (*8*, *25*−*29*). It has been suggested that steric crowding from the distal Leu 16 residue located directly above the AXCP heme iron (Figure 1D) might force the Fe−N−O unit of the 6c-NO intermediate into a distorted and unstable conformation (*27*). In this scenario, the 6c-NO → 5c-NO conversion is driven by the alleviation of unfavorable steric interactions between the Fe−NO and the distal heme pocket, since the NO binds to the proximal face in the 5c-NO species.

Aside from AXCP, the location of heme-bound NO (proximal vs distal) in other cytochromes *c*′ has yet to be definitively established. However, it is known that the ratio of 5c-NO and 6c-NO species varies widely in different types of cytochrome *c*′. For example, the ferrous-nitrosyl complex of AXCP is almost entirely 5c-NO under equilibrium conditions, whereas that of *Rhodobacter capsulatus* cytochrome *c*′ (RCCP) is reported to be a mixture of approximately equal proportions of 5c-NO and 6c-NO species (*9*). The heme center of RCCP differs from that of AXCP in that the residue located immediately above the distal coordination site is a Phe (rather than a Leu) (Figure 1C). The existence of an aromatic distal residue places RCCP in the group 1 category of cytochromes *c*′ (*30*), whereas AXCP is a group 2 cytochrome *c*′ on account of its distal Leu residue (Figure 1D). Consistent with these classifications, RCCP has a solvent-accessible channel to the distal heme pocket, whereas AXCP does not (Figure 1A,B).

To investigate how heme-NO reactivity is controlled in cytochromes *c*′, the heme coordination chemistry of RCCP has been compared with that of AXCP using optical absorption and resonance Raman (RR) spectroscopy. Overall, our results suggest that RCCP has a much more accessible distal pocket than AXCP. A model is proposed in which the heme-nitrosyl coordination number of cytochromes *c*′ could be determined by the degree of steric accessibility of the distal coordination site, rather than the Fe−His bond strength.

MATERIALS AND METHODS

RCCP and AXCP were purified using procedures similar to those described previously (*18*, *31*, *32*). Heme concentrations were determined from electronic absorption measurements using previously reported absorptivities. Optical absorption spectra were recorded using a Cary 50 spectrophotometer complete with a thermostated cell holder. Protein concentrations for absorption measurements were typically ∼2−5 μM in heme. Reduction to the ferrous state was achieved under anaerobic conditions by the addition of an ∼5-fold excess of sodium dithionite solution. ^{12}CO (CP grade, Air Products) and ^{13}CO (99% ^{13}C, Cambridge Isotope Laboratory) adducts were prepared by injecting ∼1 mL of gas through a septum sealed capillary containing argon-purged reduced protein (∼50 μL). NO adducts were prepared in a similar manner using ^{14}NO (Aldrich) or ^{15}NO (98% ^{15}N, Cambridge Isotope Laboratory) gas which had been bubbled through 0.1 M KOH solution to remove higher oxides of nitrogen. Heme-NO and heme-CO complexes were equilibrated at room temperature for 20 min prior to spectroscopic measurements. Imidazole binding to cytochrome *c*′ was examined at 25 °C by microliter additions from an imidazole stock solution at pH 8.9 containing 50 mM CHES and 0.1 M NaCl. The absorption spectrum of free imidazole was subtracted from the protein spectrum prior to each measurement.

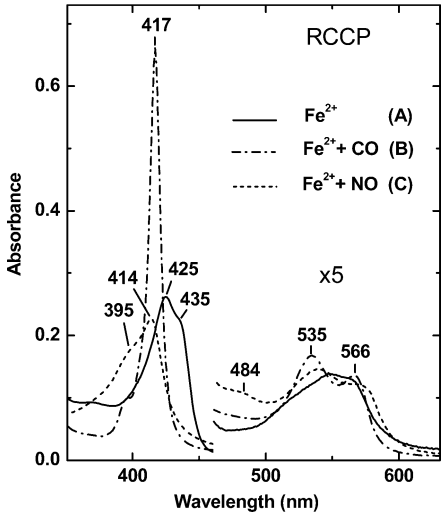

FIGURE 2: Optical absorption spectra of RCCP solutions containing ferrous (A), ferrous-carbonyl (B), and ferrous-nitrosyl (C) forms of RCCP in 50 mM phosphate buffer, pH 7.0 at 298 K. All solutions contained identical concentrations of protein (~2 μM in heme).

RR spectra of RCCP solutions, typically containing ~100 μM protein (in heme) in pH 7.0 phosphate buffer, were recorded on a custom McPherson 2061/207 spectrograph (set to 0.67 m) equipped with a Princeton Instruments liquid N_2 cooled (LN-1100PB) CCD detector and Kaiser supernotch filters. Excitation wavelengths were provided by the 413.1, 406.7, and 351.1 nm lines of a Kr ion laser (Innova) or the 441.6 nm line of a He−Cd laser (Liconix 4240NB) using laser powers of 5−20 mW at the sample (~0.03 mW for CO adducts). RR spectra were obtained in a backscattering geometry for samples contained in NMR tubes (NO complexes), or else a 90° scattering from samples contained in glass capillaries (ferrous heme and CO complexes). Photodissociation of gaseous ligands was minimized by the use of either a spinning cell (backscattering geometry) or reciprocating translation stage (90° scattering). Frozen samples were contained within NMR tubes maintained at 90 K using a liquid N_2 dewar. Frequencies were calibrated relative to indene, aspirin, CCl_4, and CD_3CN as standards and are accurate to ± 1 cm^{-1}. Optical absorption spectra of samples in their RR cells were checked before and after laser illumination using a modified Cary 50 spectrophotometer.

RESULTS

Ferrous RCCP. The UV−vis absorption spectrum of ferrous RCCP is typical of other cytochromes *c*′, featuring a split Soret band with λ_{max} 425 nm and 435 nm shoulder, together with a broad $\alpha\beta$ envelope centered near 550 nm (Figure 2). Spectroscopic data indicate that this band splitting does not arise from sample heterogeneity. Instead, the split nature of the cytochrome *c*′ Soret band has been attributed to a nondegenerate Soret electronic transition arising from electronic inequivalency in the *x*, *y* directions of the porphyrin chromophore (*33*). Room-temperature RR spectra of ferrous RCCP, obtained with 413.1 nm excitation, exhibit vibrations in the 1300−1650 cm^{-1} region that are characteristic of a 5c-Fe^{2+} high-spin heme (Figure 3 spectrum A, and Table 1), including ν_4 (1351 cm^{-1}), ν_3 (1470 cm^{-1}), ν_2 (1575 cm^{-1}), and ν_{10} (1604 cm^{-1}). Similar RR frequencies, including the relatively high frequency of the ν_2 mode, have been reported

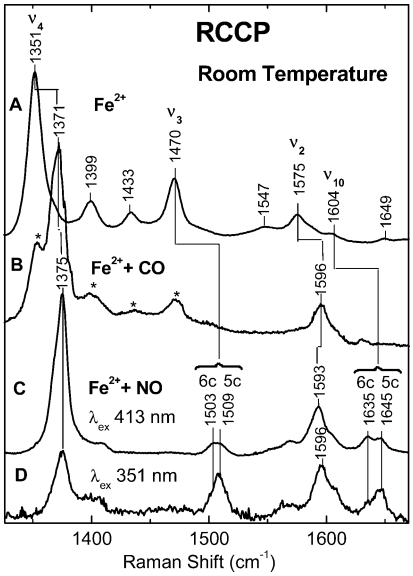

FIGURE 3: High-frequency RR spectra of RCCP in its ferrous (A), ferrous-carbonyl (B), and ferrous-nitrosyl (C and D) states. Spectra were obtained at room temperature from solutions of ~100 μM heme in 50 mM phosphate buffer, pH 7.0, using 413.1 nm excitation except for spectrum D, which was obtained using 351.1 nm excitation. Laser power at the sample was ~10 mW for ferrous RCCP, ~15 mW for the NO complex, and 0.03 mW for the CO complex. Asterisks denote minor contributions from ferrous RCCP produced by sample photodissociation in the laser beam. Photodissociation was minimized by the use of a reciprocal translation stage (CO complex), or spinning NMR tube (NO complex).

Table 1: Resonance Raman Frequencies (cm^{-1}) for Ferrous Cytochromes *c*′ and Other Five-Coordinate Ferrous Heme Proteins[a]

protein	temp, K	ν_4	ν_3	ν_2	ν_{10}	ν(Fe−His)	ref
RCCP	rt	1351	1470	1575	1604	227	this work
AXCP	rt	1351	1469	1577	1603	231	(*8*)
RMCP	293	1354	1468	1573	1604	228	(*7*)
RSCP	293	1354	1468	1573	1604	231	(*7*)
CVCP	285	1352	1469	nr[b]	nr	231	(*34*)
Mb	nr	1357	1471	1563	1607	220	(*58*)
sGC	283−293	1358	1471	1562	1606	204	(*59*)

[a] AXCP, *Alcaligenes xylosoxidans*; RMCP, *Rhodospirillum molischianum*; RSCP, *Rhodobacter sphaeroides*; CVCP, *Chromatium vinosum*; Mb, myoglobin, sGC, soluble guanylate cyclase. [b] Not reported.

for other cytochromes *c*′ (Table 1) (*7*, *8*, *33*−*35*). Figure 4 (spectrum A) shows the low-frequency RR spectrum of ferrous RCCP obtained at 441.6 nm, an excitation wavelength known to favor the enhancement of ν(Fe−His) vibrations. The ν_7 mode of ferrous RCCP is apparent at 682 cm^{-1} together with a band at 227 cm^{-1} which we assign as the Fe−N(His) stretch, ν(Fe−His), on the basis of its intensity relative to the ν_7 mode, and its disappearance in the CO and NO adducts (Figure 4, spectra B and C). A ν(Fe−His) frequency near 230 cm^{-1} is a feature of all known cytochromes *c*′ (Table 1), and is ascribed to imidazolate character in the His ligand that is electrostatically stabilized by the adjacent Arg (or Lys) residue (*7*, *8*). The characteristically high ν(Fe−His) frequencies of all cytochromes *c*′ suggest that there is no direct link between their Fe−His bond strengths and their differing propensities for 5c-NO vs 6c-NO formation.

Ferrous-CO Complex. Addition of CO to ferrous RCCP generates absorption bands at 417, 535, and 566 nm, characteristic of a 6c-CO complex (Figure 2). The spectrum

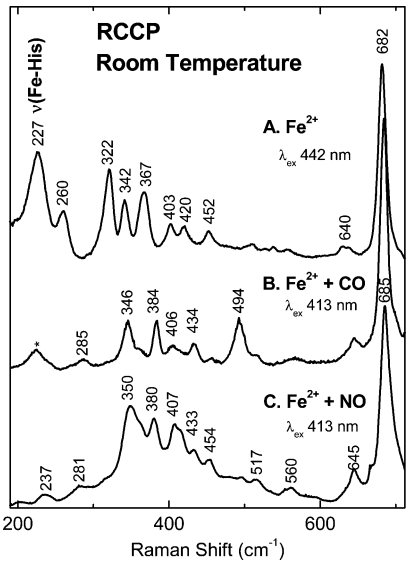

FIGURE 4: Room-temperature low-frequency RR spectra of RCCP in its ferrous (A), ferrous-carbonyl (B), and ferrous-nitrosyl (C) states. Spectra were obtained as described in Figure 3, except for spectrum A, which was obtained using 441.6 nm excitation (5 mW).

Table 2: Resonance Raman and Infrared Frequencies (cm^{-1}) of the Six-Coordinate CO Adducts of Cytochromes *c′*

	ν_4	ν_2	ν_{10}	ν(Fe−CO)	δ(Fe−CO)	ν(C−O)	ref
RCCP	1371	1596	no[a]	494	573	1966	this work
AXCP	1368	1596	no	491	572	1966	(*8*)
CVCP	1371	1591	no	492	565	1978	(*34*)

[a] Not observed.

is similar to that previously reported by Yoshimura et al. (*36*). Excitation at 413.1 nm yields the RR spectrum of the CO adduct (Figures 3B and Figure 4B) together with a minor contribution from 5c-Fe^{2+} heme due to the photolabile nature of the Fe−CO bond. In the high-frequency region (Figure 3B, Table 2) the predominant RR features of the CO adduct are the ν_4 oxidation-state marker band at 1371 cm^{-1} and the ν_2 mode at 1596 cm^{-1}. Substitution of ^{12}CO for ^{13}CO produces frequency shifts in the peaks at 494 (−4), 573 (−13), and 1966 (−44) cm^{-1} consistent with their assignment as ν(Fe−CO), δ(Fe−CO), and ν(C−O) respectively, as shown in Figure 5. The ν(Fe−CO) and ν(C−O) frequencies are similar to those of AXCP which occur at 491 and 1966 cm^{-1}, respectively (Table 2) (*8*). On the basis of established back-bonding correlations for 6c-CO complexes (*37*−*39*), the RR data for RCCP suggest that the CO ligand is located in a nonpolar environment, which in turn is consistent with CO binding to heme within the hydrophobic distal heme pocket.

Ferrous-NO Complex. Equilibration of ferrous RCCP with excess NO leads to a heme Soret absorption band with a maximum at 414 nm and a shoulder at 395 nm, consistent with a mixture of 6c-NO and 5c-NO species, respectively (Figure 2). Further evidence of a heme nitrosyl mixture stems from the presence of a 484 nm absorption band (characteristic of 5c-NO complexes), together with an ∼540, 570 nm doublet (characteristic of 6c-NO complexes). The absorption spectrum of the RCCP−NO adduct is similar to that previously reported by Yoshimura et al. (*9*), in which the nitrosyl mixture was estimated to be ∼45% 6c-NO and 55% 5c-NO (*40*). In the present study, a deconvolution analysis

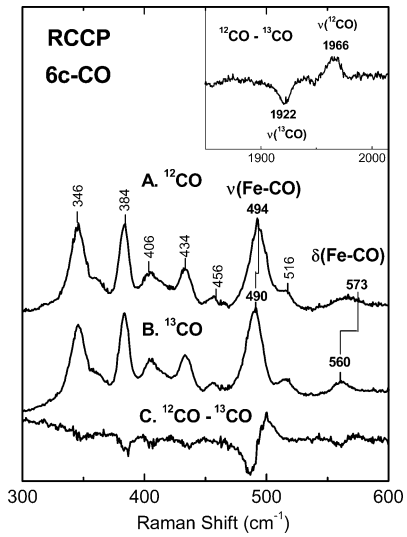

FIGURE 5: Room-temperature low-frequency RR spectra (413.1 nm excitation, 0.03 mW) for ferrous RCCP complexed with ^{12}CO (A) and ^{13}CO (B), together with the $^{12}CO - {}^{13}CO$ difference spectrum (C). The inset shows the $^{12}CO - {}^{13}CO$ difference spectrum in the high-frequency region. Other experimental conditions are as described in Figure 3.

Table 3: Resonance Raman Frequencies (cm^{-1}) of Six- and Five-Coordinate Nitrosyl Adducts of Ferrous Hemoproteins

protein	temp, K	ν_3	ν_2	ν_{10}	ν(Fe−NO)	ν(N−O)	ref
				6c-NO			
RCCP	rt	1503	1593	1635	562	no[a]	this work
RCCP	90	1506	1598	1640	569	1625	this work
AXCP	90	1504	1596	1638	579	1624	(*27*)
Mb	293	1500	1583	1635	552	1613	
HbA	rt	1500	1584	1636	551	1622	
				5c-NO			
RCCP	rt	1509	1596	1645	no	no	this work
RCCP	90	1513	1600	1651	no	no	this work
AXCP	rt	1506	1592	1641	526	1661	(*8*)
AXCP	90	1511	1596	1648	nr[b]	1661	(*27*)

[a] Not observed. [b] Not reported.

of the Soret absorption envelope (data not shown) yields an estimate for the RCCP heme-nitrosyl composition of ∼60% 6c-NO and ∼40% 5c-NO. No change in the ratio of the heme-nitrosyl populations was observed upon varying the NO concentration (0.1−2 mM), protein concentration (2−50 μM), or pH (4.0−8.9).

The RR spectrum of ferrous-nitrosyl RCCP obtained at room temperature with 413.1 nm excitation clearly reveals the presence of a mixture of 5c-NO and 6c-NO components (Figure 3C). Features specifically assigned to the 6c-NO population are observed at 1503 (ν_3), 1593 (ν_2), and 1635 cm^{-1} (ν_{10}), with vibrations at 1509 (ν_3), 1596 (ν_2), and 1645 cm^{-1} (ν_{10}) ascribed to the 5c-NO component (Table 3). Changing to 351 nm excitation, out of resonance with the 6c-NO population (λ_{max} 414 nm), produces an RR spectrum dominated by contributions from the 5c-NO population (λ_{max} 395 nm) (Figure 3D). Lowering the sample temperature to 90 K increases the relative RR intensities of the 6c-NO species at the expense of the 5c-NO species, as can be seen by comparing the 413.1 nm spectrum obtained at room temperature (Figure 3C) with that at 90 K (Figure 6A). The corresponding increase of 2−6 cm^{-1} in the porphyrin marker-band frequencies upon cooling to 90 K is consistent with a

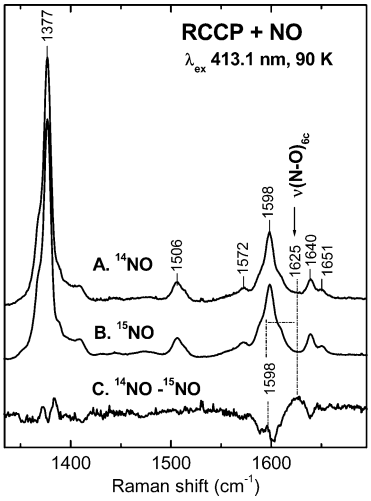

FIGURE 6: High-frequency RR spectra (413.1 nm excitation, 5 mW) obtained at 90 K for frozen solutions of ferrous RCCP complexed with ^{14}NO (A) and ^{15}NO (B), together with the ^{14}NO − ^{15}NO difference spectrum (C). Other experimental conditions are as described in Figure 3.

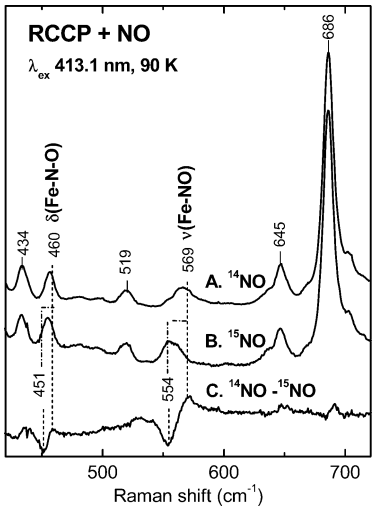

FIGURE 7: Low-frequency RR spectra (413.1 nm excitation, 5 mW) obtained at 90 K for frozen solutions of ferrous RCCP complexed with ^{14}NO (A) and ^{15}NO (B), together with the ^{14}NO − ^{15}NO difference spectrum (C). Other experimental conditions are as described in Figure 3.

contraction of the heme core, mirroring the behavior previously observed for AXCP (*8*, *27*). A sample temperature of 90 K also prevented the loss of heme-bound NO due to photodissociation in the laser beam, as previously observed for AXCP (*27*).

To facilitate the assignment of weak axial ligand vibrations in ferrous nitrosyl RCCP, experimental conditions were selected to optimize in turn the relative RR intensities of the 5c-NO and 6c-NO species. For the 6c-NO species, RR intensity was maximized using 413.1 nm excitation and a sample temperature of 90 K. Under these conditions, the ν(N−O), ν(Fe−NO), and δ(Fe−N−O) modes of the 6c-NO species are identified upon substitution of ^{14}NO with ^{15}NO from their frequency shifts at 1625 (−28), 569 (−15), and 460 (−10) cm^{-1}, respectively (Figures 6 and 7). Upon switching to room temperature, the ν(Fe−NO) and δ(Fe−NO) modes of 6c-NO RCCP are still observed, although their frequencies downshift slightly to 562 and 458 cm^{-1}, respectively (Figure 8).

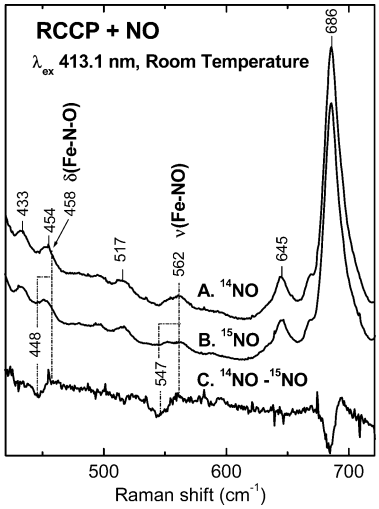

FIGURE 8: Room-temperature low-frequency RR spectra (413.1 nm excitation, 0.03 mW) of ferrous RCCP complexed with ^{14}NO (A) and ^{15}NO (B), together with the ^{14}NO − ^{15}NO difference spectrum (C). Other experimental conditions are as described in Figure 3.

The structural interpretation of axial ligand vibrations in 6c-NO hemoproteins is more complicated than for 6c-CO species (*41*). As well as being influenced by the heme pocket polarity, vibrations within the Fe−N−O unit are sensitive to mixing between the ν(Fe−NO) and δ(Fe−N−O) modes, which in turn depends on the extent to which the Fe−N−O bond angle deviates from its normal value of ∼140°. Recent density functional theory analysis of ferrous-nitrosyl complexes concluded that a clear picture of the relationship between vibrational frequencies and the heme-NO structure will require a more extensive structural database, together with improvements in computational capabilities (*41*). Nevertheless, the present study finds a significant difference between the observed ν(Fe−NO) frequencies of the RCCP and AXCP 6c-NO adducts. Whereas the RCCP 6c-NO species exhibits a fairly typical ν(Fe−NO) frequency (569 cm^{-1}), the 6c-NO intermediate of AXCP has an unusually high frequency of 579 cm^{-1}. In light of the relatively soft Fe−NO bending potential (*41*), the most likely explanation for the different frequencies would appear to lie with the Fe−N−O geometry. In line with our previous proposal (*27*), we suggest that the relatively high ν(Fe−NO) frequency in AXCP is due to a distorted Fe−N−O structure brought about by steric crowding within the distal pocket. Conversely, the more typical ν(Fe−NO) frequency of RCCP is ascribed to an Fe−N−O geometry that is less distorted than in AXCP due to a more accessible distal coordination environment. The hypothesis that RCCP has a more accessible distal coordination site than AXCP is supported by the results of our imidazole binding studies (vide infra).

Extensive efforts were made to assign the axial-ligand vibrations of the 5c-NO RCCP population. The typical frequency range for ν(Fe−NO) vibrations of 5c-NO hemoproteins is 520−530 cm^{-1}, whereas the range of ν(N−O) frequencies is approximately 1660−1680 cm^{-1} (*8*). RR measurements on ferrous-nitrosyl samples containing isotopically labeled NO were carried out using a variety of excitation wavelengths (351.1, 406.7, and 413.1 nm) and sample temperatures (90 K and room temperature). For each set of experimental conditions, the resonance enhancement of 5c-NO vibrations was confirmed via the presence of

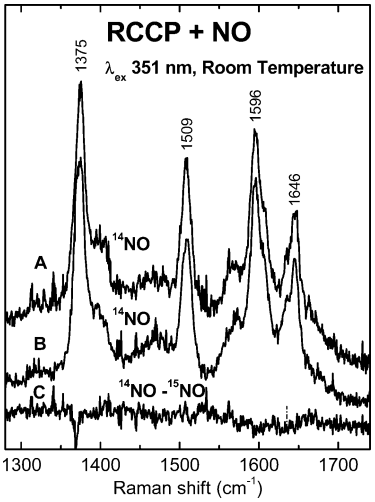

FIGURE 9: Room-temperature low-frequency RR spectra (351.1 nm excitation, 12 mW) of ferrous RCCP complexed with ^{14}NO (A) and ^{15}NO (B), together with the $^{14}NO - {}^{15}NO$ difference spectrum (C). Other experimental conditions are as described in Figure 3.

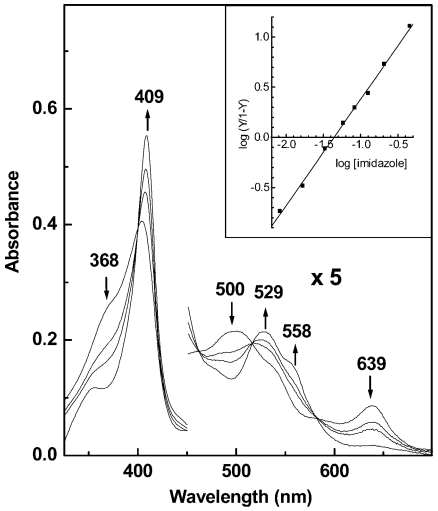

FIGURE 10: Titration of ferric RCCP with imidazole, showing representative absorption spectra of samples with imidazole concentrations of zero, 33.3 mM, 83.3 mM, and 458 mM. The concentration of ferric RCCP was ~5 μM (in heme) in 50 mM CHES (pH = 8.9) at 298 K. The inset shows a Hill plot analysis which gives K_d = 43 mM.

porphyrin marker bands characteristic of the 5c-NO species (see, for example, Figure 9). However, the apparently weak resonance enhancement of the 5c-NO axial ligand modes, as well as overlapping features from the 6c-NO species, prevented the definitive assignment of any of the 5c-NO axial ligand vibrations. Previous studies of hemoproteins have also reported difficulty in identifying ν(Fe−NO) and ν(N−O) vibrations in certain cases (see, for example, ref *42* and references therein).

Exogenous Imidazole as a Steric Probe. The use of exogenous imidazole (Im) as a probe of the steric accessibility of protein heme centers is well documented (see, for example, refs *43*−*49*). To date, no studies of Im binding to cytochromes *c*′ have been reported. In the present investigation, the ferric, ferrous, and ferrous-nitrosyl complexes of RCCP and AXCP were titrated with imidazole at pH 8.9. The optical absorption spectrum of ferric RCCP at pH 8.9 is characterized by an intense absorption band at 404 nm, together with a shoulder at ~368 nm and weaker absorption bands at ~500, 536(sh), and 639 nm, the latter being a characteristic marker of five-coordinate high-spin ferric heme. Titration of ferric RCCP with Im at pH 8.9 leads to the appearance of absorbance maxima at 409, 529, and 558-(sh) nm (Figure 10), consistent with the formation of a six-coordinate low-spin ferric heme with Im bound at the distal position (*43*, *49*). Isosbestic points (400, 462, 516, and 582 nm) observed throughout the titration are consistent with an equilibrium between two spectroscopically distinct species (ferric RCCP and its Im complex). A Hill plot analysis (Figure 10 inset) shows that Im binds noncooperatively to ferric RCCP (K_d = 43 mM) with an affinity similar to that of Im binding to sperm whale myoglobin (K_d = 28 mM) (*44*). No binding of exogenous Im was observed with 5c-Fe^{2+} RCCP, consistent with the low affinities typical of ferrous heme centers. However, the addition of Im to ferrous-nitrosyl RCCP causes the proportion of 6c-NO species to increase relative to the 5c-NO species (data not shown), consistent with Im binding trans to the NO ligand to give a 6c-NO(Im) complex. Since the 6c-NO(Im) complex has neither of its axial ligands covalently bound to the polypeptide, it is possible that either the NO or the Im ligand could occupy the distal position, with the other ligand bound to the opposite heme face.

In stark contrast to RCCP, solutions of ferric AXCP at pH 8.9 exhibit no apparent heme-Im binding in the presence of up to 1 M Im. There is also no evidence of heme-Im binding to the 5c-Fe^{2+} and 5c-NO forms of AXCP. However, when ferric AXCP is exposed to Im concentrations greater than 1 M, there is an abrupt change in optical absorption (complete upon the addition of 2 M Im) to give a spectrum resembling that of the six-coordinate RCCP ferric-Im complex shown in Figure 10 (Soret maximum at 409 nm, together with weaker features near 529 and 558 nm). The dramatic onset of heme-Im binding in AXCP above ~1 M Im suggests that this is a concentration threshold beyond which Im is able to induce protein conformation changes that allow Im to coordinate at the distal heme site. A similar type of behavior is observed for ferric AXCP at pH 7.0, wherein there is no apparent heme-Im binding for ligand concentrations up to 0.5 M, followed by abrupt conversion to the heme-Im complex as [Im] is increased to 1.5 M. It is noted that ferric AXCP exhibits a pH-dependent spin state equilibrium (pK_a ~7) between a five-coordinate high-spin form at alkaline pH and a quantum mechanically admixed high-spin/intermediate-spin state at low pH. However, the apparent lack of Im binding to ferric AXCP at both pH 8.9 and pH 7.0 with [Im] < 0.5 M appears to rule out spin-state effects as the reason for the low Im affinity of AXCP.

In summary, RCCP and AXCP exhibit very different Im binding behavior. The fact that ferric RCCP readily binds Im with a K_d of 43 mM demonstrates that Im binding to heme is much more favorable than in AXCP which exhibits no apparent complex formation in the presence of 0.5 M Im. The significantly greater Im-binding affinity of RCCP relative to AXCP is consistent with RCCP having a much more accessible distal coordination site.

DISCUSSION

Comparison of Heme Accessibility in RCCP and AXCP. The present study reveals significant differences between the

coordination chemistry of RCCP (a group 1 cytochrome *c*′) and AXCP (a group 2 cytochrome *c*′) consistent with RCCP having a more accessible distal heme coordination site. In particular, the significantly greater imidazole-binding affinity of RCCP relative to AXCP suggests that the distal coordination site in RCCP is much more sterically accessible than in AXCP. Previous ligand-binding studies have noted a similar trend in distal heme accessibility of group 1 and group 2 cytochromes *c*′. For instance, the binding affinity of ferrous heme for ethylisocyanide is 3 orders of magnitude greater for group 1 cytochromes *c*′ than for their group 2 counterparts (*50*). The variation in binding affinities between group 1 and group 2 cytochromes *c*′ diminishes as the size of the exogenous ligand decreases, consistent with smaller ligands experiencing less steric hindrance (*50*).

What structural features are responsible for making the distal coordination site of RCCP more accessible to exogenous ligands compared to that of AXCP? One factor might be the protein channel in RCCP that connects the distal heme pocket to the solvent, a feature common to all group 1 members. Alternatively, the ligand binding properties of RCCP and AXCP might depend on the immediate environment of their distal heme pockets. A notable difference between the two proteins is that RCCP has a Phe residue in its distal pocket, whereas AXCP has a Leu (Figure 1). The relative sizes of these two residues alone cannot account for the RCCP heme pocket being more accessible since the overall volume of a Phe side chain (133.9 mL/mol) is actually greater than that of a Leu (100.1 mL/mol) (*51*). Rather, steric accessibility may depend on the degree to which distal residues can adjust their conformations to allow coordination of exogenous ligands. For example, CO binding to ferrous AXCP is associated with a 134° rotation about the $C_\alpha-C_\beta$ bond of Leu16, which in turn flattens the heme group by pushing on pyrrole ring A (*25*). More extensive rearrangements are observed in ferrous RCCP upon binding *n*-butylisocyanide (BIC), including displacement of Phe 14 by rotations of 140° and 63° around the $C_\alpha-C_\beta$ and $C_\beta-C_\gamma$ bonds, respectively, as well as significant rearrangements in at least three other distal residues (*52*). It is not known whether the more extensive conformational changes observed in RCCP compared to AXCP are simply the result of BIC being a larger ligand than CO, or whether they indicate a more flexible distal pocket in RCCP compared to AXCP. Further insights into the issue of heme pocket accessibility in cytochromes *c*′ are expected from ligand-binding studies of site-directed mutants currently being prepared in our laboratories.

In contrast to its low affinity for exogenous imidazole, AXCP readily forms complexes with the smaller diatomic ligands, CO and NO. The 6c-CO complexes of AXCP and RCCP have almost identical spectroscopic properties, suggesting that both proteins bind CO in a similar fashion within their hydrophobic distal pockets. In contrast, RCCP and AXCP interact very differently with NO. Ferrous RCCP reacts with NO to yield a mixture of 6c-NO and 5c-NO species in approximately equal proportions, whereas AXCP forms a transient 6c-NO complex that subsequently converts to a predominantly 5c-NO species. The RR spectra of the 6c-NO species of the two proteins are very different. Most notably, the ν(Fe−NO) frequency of the 6c-NO species in RCCP is 10 cm^{-1} lower than that of the 6c-NO AXCP intermediate. It is conceivable that the relatively high ν(Fe−NO) frequency of the 6c-NO AXCP intermediate reflects a distorted Fe−N−O geometry brought about by a high degree of steric crowding within the distal pocket. The soft bending potential of Fe−NO relative to Fe−CO (*41*) may account for why the 6c-NO species of RCCP and AXCP are so different, and yet the 6c-CO complexes are so similar.

Structural Determinants of Heme-Nitrosyl Coordination Number. Traditionally, the formation of 5c-NO species has been linked to a weak Fe−His bond in the 5c-Fe^{2+} state, as reflected in a low ν(Fe−His) frequency. However, both RCCP and AXCP have relatively high ν(Fe−His) values, and yet are still able to form 5c-NO species. Moreover, the ν(Fe−His) frequency of RCCP is actually 4 cm^{-1} lower than that of AXCP, despite its forming a lower percentage of 5c-NO species than AXCP. The relatively high ν(Fe−His) frequency of RCCP would appear to rule out spontaneous dissociation of a weak Fe−His bond as the structural determinant of 5c-NO formation. However, it should be pointed out that if the proximal His ligand of cytochromes *c*′ were to lose its imidazolate character upon forming a 6c-NO species, the Fe−His bond may be sufficiently weakened to spontaneously dissociate to give the 5c-NO species (*8*, *27*). Nevertheless, the present study raises the distinct possibility that factors other than the Fe−His bond strength determine the heme-nitrosyl coordination number in cytochromes *c*′. Interestingly, studies of prokaryotic sGC-like heme domains have provided evidence that distal effects can influence the heme-nitrosyl coordination, although the exact mechanism remains unclear (*10*, *53*).

Because 6c-NO complexes containing a proximal His ligand must, by definition, contain NO at the distal position, it follows that steric crowding within the distal pocket will tend to disfavor their formation. The question then becomes, how might steric crowding selectively destabilize 6c-NO complexes relative to their 5c-NO counterparts? One way in which this might happen is if the 5c-NO species could bind NO in a distinct (and more thermodynamically favorable) heme environment that is not accessible to the 6c-NO state. In the case of AXCP, this alternative NO-binding environment is the proximal heme face, which is less crowded than the distal pocket, and also contains Arg 124 as an available H-bond donor (*25*). Previous studies on the AXCP 5c-NO adduct established the proximal location of NO using X-ray crystallography (*25*), with subsequent confirmation by RR spectroscopy in the solution phase (*8*). In addition, kinetic studies of NO binding to AXCP are consistent with a mechnanism in which a proximal 5c-NO species is formed via a distal 6c-NO intermediate (*27*). The present spectroscopic study of RCCP provides no direct evidence for the location (proximal or distal) of the NO ligand in the 5c-NO RCCP population. Therefore, the possibility of proximal heme-NO binding in RCCP, along with its potential role in 5c-NO formation, remains an open question.

Is there any other evidence that steric crowding favors 5c-NO formation? Yoshimura et al. have surveyed the NO binding properties of a number of group 1 and group 2 cytochromes *c*′ including AXCP, RCCP, *Rhodospirillum rubrum* cytochrome *c*′ (RRCP), *Chromatium vinousm* cytochrome *c*′ (CVCP), and *Rhodopseudomonas palustris* cytochrome *c*′ (RPCP) (*9*). Interestingly, the ferrous-nitrosyl complexes of group 1 cytochromes *c*′ tend to have a higher

percentage of 6c-NO species than group 2 cytochromes *c*′, consistent with distal pocket steric crowding being a determinant of heme-nitrosyl coordination number. Among the cytochromes *c*′ surveyed, those with the highest equilibrium ratios of 6c-NO species were the group 1 proteins RCCP (45%) and CVCP, (34%), whereas the lowest percentages of 6c-NO species were found in the group 2 proteins AXCP (<10%) and RRCP (<10%). The exception was RPCP (a group 2 cytochrome *c*′) in which the 6c-NO population was estimated to be 42%. However, RPCP is unique in that it is the only known cytochrome *c*′ to exist entirely as a monomer, rather than a homodimer.

The connection (if any) between NO binding to cytochromes *c*′ and their quaternary structure is unknown. However, CVCP is reported to undergo dimer dissociation in the presence of CO (*50*, *54*−*56*). Previous studies of CO binding to AXCP have not detected any ligand-induced dimerization (*53*). Similarly, CO does not induce subunit dissociation in RCCP (*52*, *57*). However, it has been reported that the native RCCP protein can exist in solution as a monomer/dimer mixture (*52*, *57*). In this case it is conceivable that the monomer and dimer forms of RCCP might react differently with NO, and that its heme-nitrosyl coordination number could depend on the oligomeric state of the protein.

To summarize, previous studies have correlated 5c-NO formation in hemoproteins with a weak Fe−His bond. While this appears to be true for many hemoproteins, there are a number of apparent exceptions, including cytochromes *c*′. Data from the present study point to a novel determinant of heme-nitrosyl coordination number in cytochromes *c*′ that does not depend on the Fe−His bond strength. The equilibrium ratio of 5c-NO to 6c-NO species in AXCP is significantly higher than in RCCP, despite both proteins having relatively high ν(Fe−His) frequencies of ∼230 cm^{-1}, suggesting that the extent of 5c-NO formation does not necessarily correlate with a weak Fe−His bond. Instead, RCCP appears to have a much more accessible distal heme coordination site than AXCP, on the basis of its significantly higher affinity for exogenous imidazole. The lower ν(Fe−NO) frequency of the 6c-NO RCCP species (569 cm^{-1}) relative to the 6c-NO AXCP intermediate (579 cm^{-1}) is also attributed to RCCP having a more accessible distal heme face. A model is proposed in which increased steric hindrance to distal ligand binding acts to destabilize the 6c-NO complex in favor of the 5c-NO species. Recent studies have shown that 6c-NO → 5c-NO conversion in AXCP is associated with NO changing its heme coordination site from the crowded distal pocket to the more exposed proximal heme face. Although the NO-binding location of the 5c-NO species in RCCP is still unknown, the present comparison of RCCP with AXCP supports a correlation between greater distal heme accessibility and a higher 6c-NO to 5c-NO ratio. Future NO-binding studies on site-directed mutants of cytochrome *c*′ will allow the relative influence of heme accessibility and Fe−His bond strength to be addressed in more detail, together with the issue of proximal vs distal NO binding and the affect of quaternary structure.

REFERENCES

1. Denninger, J. W., and Marletta, M. A. (1999) Guanylate cyclase and the NO/cGMP signaling pathway, *Biochim. Biophys. Acta 1411*, 334−350.
2. Poole, R. K., and Hughes, M. N. (2000) New functions for the ancient globin family: bacterial responses to nitric oxide and nitrosative stress, *Mol. Microbiol. 36*, 775−783.
3. Wasser, I. M., de Vries, S., Moënne-Loccoz, P., Schröder, I., and Karlin, K. D. (2002) Nitric oxide in denitrification: Fe/Cu metalloenzyme and metal complex NO_x redox chemistry, *Chem. Rev. 102*, 1201−1234.
4. Zhao, Y., Brandish, P. E., Ballou, D. P., and Marletta, M. A. (1999) A molecular basis for nitric oxide sensing by soluble guanylate cyclase, *Proc. Natl. Acad. Sci. U.S.A. 96*, 14753−14758.
5. Ballou, D. P., Zhao, Y., Brandish, P. E., and Marletta, M. A. (2002) Revisiting the kinetics of nitric oxide (NO) binding to soluble guanylate cyclase: the simple NO-binding model is incorrect, *Proc. Natl. Acad. Sci. U.S.A. 99*, 12097−12101.
6. Schelvis, J. P. M., Seibold, S. A., Cerda, J. F., Garavito, R. M., and Babcock, G. T. (2000) Interaction of nitric oxide with prostaglandin endoperoxide H synthase-1: implications for Fe−His bond cleavage in heme proteins, *J. Phys. Chem. B 104*, 10844−10850.
7. Othman, S., Richaud, P., Verméglio, A., and Desbois, A. (1996) Evidence for a proximal histidine interaction in the structure of cytochromes *c*′ in solution: a resonance Raman study, *Biochemistry 35*, 9224−9234.
8. Andrew, C. R., Green, E. L., Lawson, D. M., and Eady, R. R. (2001) Resonance Raman studies of cytochrome *c*′ support the binding of CO and NO to opposite sides of the heme: implications for ligand discrimination in heme-based sensors, *Biochemistry 40*, 4115−4122.
9. Yoshimura, T., Fujii, S., Kamada, H., Yamaguchi, K., Suzuki, S., Shidara, S., and Takakuwa, S. (1996) Spectroscopic characterization of nitrosylheme in nitric oxide complexes of ferric and ferrous cytochrome *c*′ from photosynthetic bacteria, *Biochim. Biophys. Acta 1292*, 39−46.
10. Karow, D. S., Pan, D., Tran, R., Pellicena, P., Presley, A., Mathies, R. A., and Marletta, M. (2004) Spectroscopic characterization of the soluble guanylate cyclase-like heme domains from *Vibrio cholerae* and *Thermoanaerobacter tengcongensis*, *Biochemistry 43*, 10203−10211.
11. Meyer, T. E., and Kamen, M. D. (1982) New perspectives on *c*-type cytochromes, *Adv. Protein Chem. 35*, 105−212.
12. Moore, G. R., and Pettigrew, G. W. (1990) *Cytochromes c; Evolutionary, Structural and Physicochemical Aspects*, Springer-Verlag, Berlin.
13. Yoshimura, T., Iwasaki, H., Shidara, S., Suzuki, S., Nakahara, A., and Matsubura, T. (1988) Nitric oxide complex of cytochrome *c*′ in cells of denitrifying bacteria, *J. Biochem. 103*, 1016−1019.
14. Yoshimura, T., Shidara, S., Ozaki, T., and Kamada, H. (1993) 5-coordinated nitrosylhemoprotein in the whole cells of denitrifying bacterium, *Achromobacter xylosoxidans* NCIB 11015, *Arch. Microbiol. 160*, 498−500.
15. Ferguson, S. J. (1991) The functions and synthesis of bacterial *c*-type cytochromes with a particular reference to *Paracoccus denitrificans* and *Rhodobacter capsulatus*, *Biochim. Biophys. Acta 1058*, 17−20.
16. Moir, J. W. B. (1999) Cytochrome *c*′ from *Paracoccus denitrificans*: spectroscopic studies consistent with a role for the protein in nitric oxide metabolism, *Biochim. Biophys. Acta 1430*, 65−72.
17. Cross, R., Aish, J., Paston, S. J., Poole, R. K., and Moir, J. W. B. (2000) Cytochrome *c*′ from *Rhodobacter capsulatus* confers increased resistance to nitric oxide, *J. Bacteriol. 182*, 1442−1447.
18. Cross, R., Lloyd, D., Poole, R. K., and Moir, J. W. B. (2001) Enzymatic removal of nitric oxide catalyzed by cytochrome *c*′ in *Rhodobacter capsulatus*, *J. Bacteriol. 183*, 3050−3054.
19. Anjum, M. F., Stevanin, T. M., Read, R. C., and Moir, J. W. B. (2002) Nitric oxide metabolism in *Neisseria* meningitidis, *J. Bacteriol. 184*, 2987−2993.
20. Ambler, R. P., Bartsch, R. G., Daniel, M., Kamen, M. D., McLellan, L., Meyer, T. E., and Van Beeumen, J. (1981) Amino acid sequences of bacterial cytochromes *c*′ and *c-556*, *Proc. Natl. Acad. Sci. U.S.A. 78*, 6854−6857.
21. Ramirez, L. M., Axelrod, H. L., Herron, S. R., Rupp, B., Allen, J. P., and Kantardjieff, K. A. (2003) High-resolution crystal structure of ferricytochrome *c*′ from *Rhodobacter sphaeroides*, *J. Chem. Crystallogr. 33*, 413−424.
22. Dobbs, A. J., Anderson, B. F., Faber, H. R., and Baker, E. N. (1996) Three-dimensional structure of cytochrome *c*′ from two *Alcaligenes* species and the implications for four-helix bundle structures, *Acta Crystallogr. D 52*, 356−368.

23. Archer, M., Banci, L., Dikaya, E., and Romão, M. J. (1997) Crystal structure of cytochrome *c*′ from *Rhodocyclus gelatinosus* and comparison with other cytochromes *c*′, *J. Biol. Inorg. Chem. 2*, 611−622.
24. Shibata, N., Satoaki, I., Misaki, S., Meyer, T. E., Bartsch, R. G., Cusanovich, M. A., Morimoto, Y., Higuchi, Y., and Yasuoka, N. (1998) Basis for monomer stabilization in *Rhodopseudomonas palustris* cytochrome *c*′ derived from the crystal structure, *J. Mol. Biol. 284*, 751−760.
25. Lawson, D. M., Stevenson, C. E. M., Andrew, C. R., and Eady, R. R. (2000) Unprecedented proximal binding of nitric oxide to heme: implications for guanylate cyclase, *EMBO J. 19*, 5661−5671.
26. George, S. J., Andrew, C. R., Lawson, D. M., Thorneley, R. N. F., and Eady, R. R. (2001) Stopped-flow infrared spectroscopy reveals a six-coordinate intermediate in the formation of the proximally bound five-coordinate NO adduct of cytochrome *c*′, *J. Am. Chem. Soc. 123*, 9683−9684.
27. Andrew, C. R., George, S. J., Lawson, D. M., and Eady, R. R. (2002) Six- to five-coordinate heme-nitrosyl conversion in cytochrome *c*′ and its relevance to guanylate cyclase, *Biochemistry 41*, 2353−2360.
28. Lawson, D. M., Stevenson, C. E. M., Andrew, C. R., George, S. J., and Eady, R. R. (2003) A two-faced molecule offers NO explanation: the proximal binding of nitric oxide to haem, *Biochem. Soc. Trans. 31*, 553−557.
29. Andrew, C. R., Rodgers, K. R., and Eady, R. R. (2003) A novel kinetic trap for NO release from cytochrome *c*′: a possible mechanism for NO release from activated soluble guanylate cyclase, *J. Am.* Chem. Soc. *125*, 9548−9549.
30. Tahirov, T. H., Misaki, S., Meyer, T. E., Cusanovich, M. A., Higuchi, Y., and Yasuoka, N. (1996) High-resolution crystal structures of two polymophs of cytochrome *c*′ from the purple phototrophic bacterium *Rhodobacter capsulatus*, *J. Mol. Biol. 259*, 467−479.
31. Ambler, R. P. (1973) The amino acid sequence of cytochrome *c*′ from *Alcaligenes* sp. NCIB 11015, *Biochem. J. 1345*, 751−758.
32. Norris, G. E., Anderson, B. F., Baker, E. N., and Rumball, S. V. (1979) Purification and preliminary crystallographic studies on azurin and cytochrome *c*′ from *Alcaligenes denitrificans* and *Alcaligenes sp*. NCIB 11015, *J. Mol. Biol. 135*, 309−312.
33. Strekas, T. C., and Spiro, T. G. (1974) Resonance-Raman evidence for anomalous heme structures in cytochrome *c*′ from *Rhodopseudomonas palustris*, *Biochim. Biohys. Acta 351*, 237−245.
34. Hobbs, J. D., Larsen, R. W., Meyer, T. E., Hazzard, J. H., Cusanovich, M. A., and Ondrias, M. R. (1990) Resonance Raman characterization of *Chromatium vinosum* cytochrome *c*′. Effect of pH and comparison of equilibrium and photolyzed carbon monoxide species, *Biochemistry 29*, 4166−4174.
35. Kitagawa, T., Ozaki, Y., Kyooku, Y., and Horio, T. (1977) Resonance Raman study of the pH-dependent and detergent-induced structural alterations in the heme moiety of *Rhodospirillum rubrum* cytochrome *c*′, *Biochim. Biophys. Acta 495*, 1−11.
36. Yoshimura, T., Suzuki, S., Iwasaki, H., and Takakuwa, S. (1987) Spectral properties of cytochrome *c*′ from *Rhodopseudomonas capsulatus* B100 and its CO complex, *Biochem. Biophys. Res. Commun. 144*, 224−231.
37. Li, T. S., Quillin, M. L., Phillips, G. N., and Olson, J. S. (1994) Structural determinants of the stretching frequency of CO bound to myoglobin, *Biochemistry 33*, 1433−1446.
38. Li, X. Y., and Spiro, T. G. (1988) Is bound CO linear or bent in heme proteins? Evidence from resonance Raman and infrared spectroscopic data, *J. Am. Chem. Soc. 110*, 6024−6033.
39. Ray, G. B., Li, X. Y., Ibers, J. A., Sessler, J. L., and Spiro, T. G. (1994) How far can proteins bend the FeCO unit? Distal polar and steric effects in heme proteins and models, *J. Am. Chem. Soc. 116*, 162−176.
40. Yoshimura, T., Suzuki, S., Iwasaki, H., and Takakuwa, S. (1987) Spectral properties of nitric oxide complex from cytochrome *c*′ from *Rhodopseudomonas capsulata* B100, *Biochem. Biophys. Res. Commun. 145*, 868−875.
41. Coyle, C. M., Vogel, K. M., Rush, I., Thomas S., Kozlowski, P. M., Williams, R., and Spiro, T. G. (2003) FeNO structure in distal pocket mutants of myoglobin based on resonance Raman spectroscopy, *Biochemistry 42*, 4896−4903.
42. Lukat-Rodgers, G. S., and Rodgers, K. R. (1997) Characterization of ferrous FixL-nitric oxide adducts by resonance Raman spectroscopy, *Biochemistry 36*, 4178−4187.
43. Winkler, W. C., Gonzalez, G., Wittenberg, J. B., Hille, R., Dakappagari, N., Jacob, A., Gonzalez, L. A., and Gilles-Gonzalez, M. A. (1996) Nonsteric factors dominate binding of nitric oxide, azide, imidazole, cyanide, and fluoride to the Rhizobial heme-based oxygen sensor FixL, *Chem. Biol. 3*, 841−850.
44. Mansy, S. S., Olson, J. S., Gonzalez, G., and Gilles-Gonzalez, M. A. (1998) Imidazole is a sensitive probe of steric hindrance in the distal pockets of oxygen-binding heme proteins, *Biochemistry 37*, 12452−12457.
45. Dumortier, C., Holt, J. M., Meyer, T. E., and Cusanovich, M. A. (1998) Imidazole binding to *Rhodobacter capsulatus* cytochrome c_2, *J. Biol. Chem. 273*, 25647−25653.
46. Decatur, S. M., Franzen, S., DePillis, G. D., Dyer, R. B., Woodruff, W. H., and Boxer, S. G. (1996) *Trans* effects in nitric oxide binding to myoglobin cavity mutant H93G, *Biochemistry 35*, 4939−4944.
47. Zhao, Y., Hoganson, C., Babcock, G. T., and Marletta, M. A. (1998) Structural changes to the heme proximal pocket induced by nitric oxide binding to soluble guanylate cyclase, *Biochemistry 37*, 12458−12464.
48. Pond, A. E., Roach, M. P., Thomas, M. R., Boxer, S. G., and Dawson, J. H. (2000) The H93G myoglobin mutant as a versatile template for modeling heme proteins: ferrous, ferric, and ferryl mixed-ligand complexes with imidazole in the cavity, *Inorg. Chem. 39*, 6061−6066.
49. Hirst, J., Wilcox, S. K., Ai, J., Möenne-Loccoz, P., Loehr, T. M., and Goodin, D. B. (2001) Replacement of the axial histidine ligand with imidazole in cytochrome *c* peroxidase. 2. Effects on heme coordination and function, *Biochemistry 40*, 1274−1283.
50. Kassner, R. J. (1991) Ligand binding properties of cytochromes *c*′, *Biochim. Biophys. Acta 1058*, 8−12.
51. Zamyatnin, A. A. (1972) Protein volume in solution, *Prog. Biophys. Mol. Biol. 24*, 107−123.
52. Tahirov, T. H., Misaki, S., Meyer, T. E., Cusanovich, M. A., Higuchi, Y., and Yusuoka, N. (1996) Concerted movement of side chains in the haem vicinity observed on ligand binding in cytochrome *c*′ from *Rhodobacter capsulatus*, *Nat. Struct. Biol. 3*, 459−464.
53. Nioche, P., Berka, V., Vipond, J., Minton, N., Tsai, A.-L., and Raman, C. S. (2004) Femtomolar sensitivity of a NO sensor from *Clostridium botulinum*, *Science 306*, 1550−1553.
54. Ren, Z., Meyer, T., and McRee, D. E. (1993) Atomic-structure of a cytochrome *c*′ with an unusual ligand-controlled dimer dissociation at 1.8 Å resolution, *J. Mol. Biol. 234*, 433−445.
55. Doyle, M. L., Gill, S. J., and Cusanovich, M. A. (1986) Ligand controlled dissociation of *Chromatium vinosum* cytochrome *c*′, *Biochemistry 25*, 2509−2516.
56. Cusanovich, M. A., and Gibson, Q. H. (1973) Anomalous ligand binding by a class of high spin *c*-type cytochromes, *J. Biol. Chem. 248*, 822−834.
57. Cusanovich, M. A. (1971) Molecular weights of some cytochromes *cc*′, *Biochim. Biophys. Acta 236*, 238−241.
58. Choi, S., Spiro, T. G., Langry, K. C., Smith, K. M., Budd, D. L., and La Mar, G. N. (1982) Structural correlations and vinyl influences in resonance Raman spectra of protoheme complexes and proteins, *J. Am. Chem. Soc. 104*, 4345−4351.
59. Deinum, G., Stone, J. R., Babcock, G. T., and Marletta, M. A. (1996) Binding of nitric oxide and carbon monoxide to soluble guanylate cyclase as observed with resonance Raman spectroscopy, *Biochemistry 35*, 1540−1547.

BI050428G